

Analytical expressions for optimum alignment modes of highly segmented mirrors

L. Noethe

European Southern Observatory, Karl-Schwarzschild-Straße 2,
D-85748 Garching bei München, Germany

Abstract

Abstract. The major sources causing deterioration of optical quality in extremely large optical telescopes are misadjustments of the mirrors, deformations of monolithic mirrors, and misalignments of segments in segmented mirrors. For active optics corrections, all three errors, which can partially compensate each other, are measured simultaneously. It is therefore of interest to understand the similarities and differences between the three corresponding types of modes which describe these errors. The first two types are best represented by Zernike polynomials and elastic modes respectively, both of them being continuous and smooth functions. The segment misalignment modes, which are derived by singular value decomposition, are by their nature not smooth and in general discontinuous. However, for mirrors with a large number of segments, the lowest modes become effectively both smooth and continuous. This paper derives analytical expressions for these modes, using differential operators and their adjoints, for the limit case of infinitesimally small segments. For segmented mirrors with approximately 1000 segments, it is shown that these modes agree well with the corresponding lowest singular value decomposition modes. Furthermore, the analytical expressions reveal the nature of the segment misalignment modes and allow for a detailed comparison with the elastic modes of monolithic mirrors. Some mathematical features emerge as identical in the two cases.

1 Introduction

The first large optical telescope with a segmented mirror was the ten-meter Keck Telescope. Its primary mirror consisted of 36 hexagonal segments. All currently envisaged extremely large optical telescopes will have segmented primary mirrors, but with a much larger number of hexagonal segments, of the order of one thousand or more. Assuming that the shapes of the segments are perfect at all times, the only source for wavefront errors generated by a segmented mirror would be misalignments of the segments. These can be measured either optically or by edge sensors at intersegment edges. Both types of measurements can, in principle, detect the relative piston and the relative tilt of adjacent segments. The misalignments are then corrected by appropriate vertical position changes of actuators which can modify piston, tip and tilt of each segment [1].

If the signals given by the measurements were free of noise and the actuators were perfect, the misalignments of the segments could be perfectly corrected. But, in reality, both signal noise and correction noise will give rise to residual misalignments. Both the signals and the actuator positions can be represented as vectors with suitable sets of base vectors. If the errors are introduced by the actuators themselves, one can choose an arbitrary orthogonal set of base vectors. However, if the errors are due to the signals, an optimum modal correction requires the possibility to expand the signal into a set of well distinguishable, that is orthogonal signal modes, which correspond to well distinguishable, that is orthogonal, actuator modes. Such modes are the optimum alignment modes. For mathematical reasons, also described in section 2, they were called normal modes in reference [1]. These modes can be calculated by Singular Value Decomposition (SVD). In the rest of the paper we assume that the actuators are perfect and noise is only introduced by the signals.

For segmented mirrors with a thousand segments or more the modes with the lowest so called singular values are rather smooth. They are also the ones which appear statistically with the largest amplitudes in an expansion of the misalignment error due to random signal noise. In modern large active optical telescopes [2] containing both segmented and flexible monolithic mirrors the lowest normal modes could largely be compensated or corrected by other elements in the telescope optics. This shows the need to compare the normal modes with other sets of modes used in large telescopes, for example Zernike polynomials or elastic modes of monolithic mirrors [3].

In the limit of an infinite number of segments over a finite area the lowest normal modes should be continuous smooth functions. If the relationship between a position function and the corresponding signal function is expressed by a continuous operator, such smooth functions can be calculated from differential equations and appropriate boundary conditions. It should therefore be possible to derive analytical expressions for the lowest normal modes in the limit of infinitesimally small segments.

Section 2 outlines the method to obtain the analytical solutions. Before treating the case of two-dimensional segmentation the method is applied in section 3 to two examples of one-dimensional line segments. In section 4 the method is used to calculate analytical expressions of the normal modes of a mirror with hexagonal segments and section 5 compares the analytical solutions with the SVD solutions of a highly segmented mirror. Section 6 discusses the relationship to modes calculated with variational methods to minimise the r.m.s. of the signal vector for a given r.m.s. of the actuator vector and section 7 shows the relationship to elastic minimum energy modes of a circular plate.

2 Method to obtain analytical solutions

A given set of actuator positions is described by a vector $\tilde{\mathbf{v}}$ in a n_{act} -dimensional vector space \mathcal{A} , and a given set of signals by a vector $\tilde{\mathbf{u}}$ in a n_{sig} -dimensional vector space \mathcal{S} . Without noise effects, that is if the signals depend only on the actuator positions, the actuator vectors are related to the signal vectors by a linear mapping A from \mathcal{A} to \mathcal{S} , represented as a two-dimensional $n_{\text{sig}} \times n_{\text{act}}$ matrix \mathbf{A} :

$$\mathbf{A}\tilde{\mathbf{v}} = \tilde{\mathbf{u}} \quad (1)$$

In this case a misalignment could be perfectly corrected by actuator changes. In reality, noise in the signals is not negligible and only those signal vectors which are in the image space of \mathcal{A} under the mapping A can be fully corrected. An optimum modal correction of a misalignment of the segments requires the possibility to expand the signal in an orthogonal set $\{\mathbf{u}_i\}$ of signal modes which are related by the mapping A to an orthogonal set $\{\mathbf{v}_i\}$ of actuator modes. Such sets are generated by the Singular Value Decomposition of \mathbf{A} :

$$\mathbf{A} = \mathbf{U}\mathbf{\Sigma}\mathbf{V}^H \quad (2)$$

\mathbf{U} is a matrix of dimension $n_{\text{sig}} \times n_{\text{act}}$ and $\mathbf{\Sigma}$ and \mathbf{V}^H , where the superscript H denotes the adjoint matrix, are square matrices of dimension $n_{\text{act}} \times n_{\text{act}}$. The matrix $\mathbf{\Sigma}$ is diagonal and contains n_{act} so called singular values $\sigma_{\text{svd},i}$. The n_{act} column vectors of \mathbf{U} and row vectors of \mathbf{V} form orthonormal sets $\{\mathbf{u}_i\}$ and $\{\mathbf{v}_j\}$, respectively, that is, with \langle, \rangle denoting the inner vector product,

$$\langle \mathbf{u}_i, \mathbf{u}_j \rangle = \langle \mathbf{v}_i, \mathbf{v}_j \rangle = \delta_{i,j} \quad (3)$$

The vectors \mathbf{u}_i and \mathbf{v}_i which are related by

$$\mathbf{A}\mathbf{v}_i = \sigma_{\text{svd},i} \mathbf{u}_i \quad (4)$$

will be called normal signal and actuator modes, respectively, since they are eigenvectors of so called normal matrices, which are matrices which commute with their adjoints. The normal matrices are $\mathbf{A}^H\mathbf{A}$ in the case of the actuator vectors and $\mathbf{A}\mathbf{A}^H$ in the case of the signal vectors. In the following the term normal mode without a specification 'actuator' or 'signal' will refer to an actuator mode.

For a large number of n_{seg} of segments the normal modes with the smallest singular values become rather smooth. In the limit of an infinite number of segments over a finite area, that is in terms of the radii a of a segment (see figure 5) and R of the mirror, $a/R \rightarrow 0$, they should converge to functions which are continuously differentiable an infinite number of times. Let L denote the continuous operator which corresponds to the matrix \mathbf{A} , and f_i and g_i the functions, called the analytical position and signal modes, to which the actuator modes \mathbf{v}_i and the signal modes \mathbf{u}_i , respectively, converge for $a/R \rightarrow 0$. The position functions f_i will also be referred to as analytical normal modes. The two now infinite sets $\{f_i\}$ and $\{g_i\}$ will have, similar to the sets

$\{\mathbf{v}_i\}$ and $\{\mathbf{u}_i\}$, the following two characteristics. Let the vector products be defined by

$$\langle f_i, f_j \rangle = \frac{1}{2D} \int_{-D}^{+D} dx f_i(x) f_j(x) = \frac{1}{2} \int_{-1}^{+1} d\xi f_i(\xi) f_j(\xi) \quad (5)$$

for the one-dimensional problems with a length of the chain of segments of $2D$ and the normalised variable $\xi = x/D$ and by

$$\langle f_i, f_j \rangle = \frac{1}{\pi(R^2 - r_1^2)} \int_0^{2\pi} d\varphi \int_{r_1}^R r dr f_i(r, \varphi) f_j(r, \varphi) = \frac{1}{\pi(1 - \rho_1^2)} \int_0^{2\pi} d\varphi \int_{\rho_1}^1 \rho d\rho f_i(\rho, \varphi) f_j(\rho, \varphi) \quad (6)$$

for the two-dimensional problems, where r is the radial, φ the azimuthal coordinate, R the outer radius of a circular mirror, r_1 the radius of its inner hole, $\rho = r/R$ the normalised radial variable, and $\rho_1 = r_1/R$ the normalised radius of the inner hole. The first characteristic is then that the two sets of functions are orthonormal, that is

$$\langle f_i, f_j \rangle = \langle g_i, g_j \rangle = \delta_{i,j} \quad (7)$$

The second characteristic is that the members f_i and g_i are related by

$$L f_i = \tilde{\sigma}_i g_i, \quad (8)$$

where the $\tilde{\sigma}_i$, which from now on will be called analytical singular values, correspond to the singular values $\sigma_{\text{svd},i}$ in the discrete SVD.

The functions f_i and g_i can be derived from the two conditions (7) and (8). Introducing equation (8) into equation (7) gives

$$\tilde{\sigma}_i^2 \langle g_i, g_j \rangle = \langle L f_i, L f_j \rangle = \tilde{\sigma}_i^2 \delta_{i,j} \quad (9)$$

After integrating the vector product $\langle L f_i, L f_j \rangle$ by parts one gets [4]

$$\langle L f_i, L f_j \rangle = \langle L^H L f_i, f_j \rangle = \langle L^F L f_i, f_j \rangle + \underline{\beta}_L[f_i, f_j], \quad (10)$$

where L^H is the adjoint of L , L^F the formal or Lagrange adjoint of L , and $\underline{\beta}_L[f_i, f_j]$ a boundary functional. If the boundary functional is zero equations (7), (9), and (10) lead to the linear differential equation

$$L^F L f = \tilde{\sigma}^2 f \quad (11)$$

Equations (10) and (11) are the fundamental equations for the derivation of the expressions for the analytical normal modes in the limit of infinitely fine segmentation. The boundary conditions which are required to derive specific infinite sets $\{f_i\}$ of analytical normal modes and the corresponding sets $\{\tilde{\sigma}_i\}$ of analytical singular values from the general solution of equation (11) are obtained from the requirement that the boundary functional vanishes. The form of the operator L^F and the boundary functional depend on the operator L . One of the problems is therefore to find the correct expression for the linear differential operator L which corresponds, in the limit of infinitely fine segmentation, to the matrix \mathbf{A} .

3 One-dimensional segmentation

The method outlined in section 2 is first applied to the mathematically easier case of one-dimensional segmentation. In addition, some of the features appearing in this section are similar to the ones occurring in the more interesting examples of two-dimensional segmentation discussed in sections 4 and 5.

3.1 SVD solutions

Figure 1 shows two examples which are based on linear chains of segments. In figure 1a each segment can only

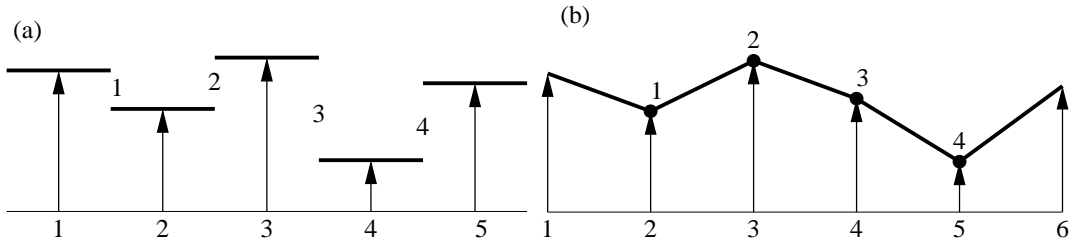


Figure 1: **(a)** : Segments with piston movements only, **(b)** : Segments linked at the interfaces.

be moved in vertical direction. If the actuator positions are denoted by z_i , the signals s_i measured by vertical displacement sensors are given by

$$s_i = z_{i+1} - z_i \quad (12)$$

In figure 1b the segments are linked and the actuators are at the links and at both ends of the chain. The signals s_i are defined by

$$s_i = z_i - 2z_{i+1} + z_{i+2} \quad (13)$$

For small angles s_i is approximately proportional to the difference between the tilts of the segments. The matrices linking the actuator positions to the signals are given by

$$\mathbf{A}_a = \begin{pmatrix} -1 & 1 & 0 & 0 & 0 \\ 0 & 1 & -1 & 0 & 0 \\ 0 & 0 & 1 & -1 & 0 \\ 0 & 0 & 0 & 1 & -1 \end{pmatrix} \quad (14)$$

for the example (a) with $n_{\text{sig}} = n_{\text{act}} - 1$ and

$$\mathbf{A}_b = \begin{pmatrix} 1 & -2 & 1 & 0 & 0 & 0 \\ 0 & 1 & -2 & 1 & 0 & 0 \\ 0 & 0 & 1 & -2 & 1 & 0 \\ 0 & 0 & 0 & 1 & -2 & 1 \end{pmatrix} \quad (15)$$

for the example (b) with $n_{\text{sig}} = n_{\text{act}} - 2$. In both examples the number n_{nz} of normal modes with non-zero singular values is equal to the number of signals.

For large values of n_{act} the lowest modes, which are the ones with the smallest singular values, approach smooth functions. Figure 2 shows for the example (b) with 100 segments the three modes with the lowest singular values.

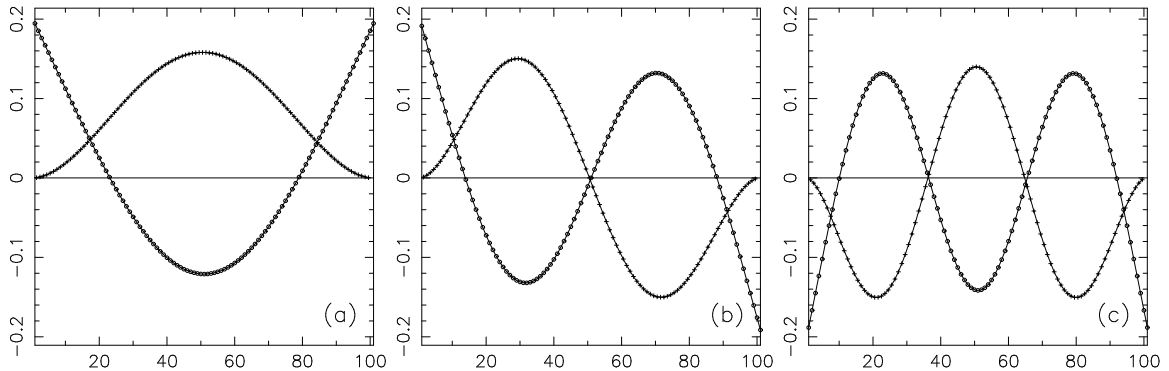


Figure 2: Example (b) : Actuator values (circles) and sensor signals (crosses) for the three SVD modes with the lowest singular values. The solid lines are the mode shapes calculated analytically for an infinite number of segments.

3.2 Analytical solutions for one-dimensional segmentation

3.2.1 Example (a)

In the limit of infinitely small segments the operator L which corresponds to the matrix \mathbf{A}_a of example (a) is given by

$$L = \frac{d}{dx} = \frac{1}{D} \frac{d}{d\xi} \quad (16)$$

Then, with $-D$ and D being the left and the right end of the chain of segments, equation (10) becomes

$$\langle Lf_i(x), Lf_j(x) \rangle = \frac{1}{2D^2} \int_{-1}^{+1} \left(\frac{d}{d\xi} f_i(\xi) \right) \left(\frac{d}{d\xi} f_j(\xi) \right) d\xi \quad (17)$$

$$= -\frac{1}{2D^2} \int_{-1}^{+1} \left(\frac{d^2}{d\xi^2} f_i(\xi) \right) f_j(\xi) d\xi + \frac{1}{2D^2} \left[\left(\frac{d}{d\xi} f_i(\xi) \right) f_j(\xi) \right]_{-1}^{+1} \quad (18)$$

For an arbitrary choice of a function f_j from the set $\{f_j\}$ the boundary functional vanishes only if

$$\left(\frac{d}{d\xi} f(\xi) \right)_{\xi=-1} = \left(\frac{d}{d\xi} f(\xi) \right)_{\xi=+1} = 0 \quad (19)$$

The differential equation (11) in terms of the normalised variable ξ is then given by

$$-\frac{1}{D^2} \frac{d^2}{d\xi^2} f(\xi) = \tilde{\sigma}^2 f(\xi), \quad (20)$$

or, with the new normalised parameter $\sigma = D\tilde{\sigma}$ which has the advantage that it is independent of the length $2D$ of the chain and has got the unit 1, by

$$-\frac{d^2}{d\xi^2} f(\xi) = \sigma^2 f(\xi) \quad (21)$$

The general solutions are either symmetric or antisymmetric :

$$f_s(\xi) = c_s \cos(\sigma\xi) \quad (22)$$

$$f_a(\xi) = c_a \sin(\sigma\xi) \quad (23)$$

with c_s and c_a denoting arbitrary constants. Introducing these equations into the boundary conditions (19) gives the equations from which the infinite sets of normalised analytical singular values $\sigma_i = D\tilde{\sigma}_i$ for the symmetric and the antisymmetric cases can be obtained. The σ_i are identical to the wavenumbers of the solution functions and given by

$$\sigma_i = i \frac{\pi}{2} \quad (24)$$

Obviously, for the symmetric and antisymmetric cases the sets $\{f_{s/a,i}\}$ and $\{Lf_{s/a,i}\}$, representing the analytical position and signal modes respectively, are orthogonal sets of functions. The following relationships, which follow from the equations (7), (9), and (17) will be required in section 3.3.1 :

$$\begin{aligned} \sigma_i^2 = D^2 \tilde{\sigma}_i^2 &= D^2 \frac{\langle Lf_i(x), Lf_i(x) \rangle}{\langle f_i(x), f_i(x) \rangle} \\ &= \int_{-1}^{+1} \left(\frac{d}{d\xi} f_i(\xi) \right)^2 d\xi / \int_{-1}^{+1} (f_i(\xi))^2 d\xi \end{aligned} \quad (25)$$

3.2.2 Example (b)

In the limit of infinitely small segments the operator L which corresponds to the matrix \mathbf{A}_b of example (b) is given by

$$L = \frac{d^2}{dx^2} = \frac{1}{D^2} \frac{d^2}{d\xi^2} \quad (26)$$

Taking the same steps as in section 3.2.1 one gets

$$L^F L = \frac{1}{D^4} \frac{d^4}{d\xi^4} \quad (27)$$

$$\underline{\beta}_L[f_i, f_j] = \frac{1}{2D^4} \left[\left(\frac{d^2}{d\xi^2} f_i \right) \frac{df_j}{d\xi} - \left(\frac{d^3}{d\xi^3} f_i \right) f_j \right]_{-1}^{+1} \quad (28)$$

The differential equation is therefore given by

$$\left(\frac{d^4}{d\xi^4} - \sigma^2 \right) f(\xi) = 0 \quad (29)$$

with $\sigma = D^2 \tilde{\sigma}$. The fourth-order differential operator in equation (29) can be factorised into two second-order differential operators :

$$\left(\frac{d^2}{d\xi^2} - \sigma \right) \left(\frac{d^2}{d\xi^2} + \sigma \right) f(\xi) = 0 \quad (30)$$

With the definition

$$\lambda^2 = \sigma \quad (31)$$

the symmetric and antisymmetric solutions are, with a_s and a_a denoting additional coefficients,

$$f_s(\xi) = c_s [\cos(\lambda\xi) + a_s \cosh(\lambda\xi)] \quad (32)$$

$$f_a(\xi) = c_a [\sin(\lambda\xi) + a_a \sinh(\lambda\xi)] \quad (33)$$

Both sets of solutions require two boundary conditions which can be derived from the boundary functional (28). This must be zero for arbitrary functions taken from the sets of functions $\{f_{s,j}\}$ or $\{f_{a,j}\}$. Since at least for some of them both the function and its derivative are non-zero at the edges the four conditions which guarantee that the boundary functional is zero for all combinations of i and j are

$$\left(\frac{d^2}{d\xi^2} f(\xi) \right)_{\xi=-1} = \left(\frac{d^2}{d\xi^2} f(\xi) \right)_{\xi=+1} = 0 \quad (34)$$

$$\left(\frac{d^3}{d\xi^3} f(\xi) \right)_{\xi=-1} = \left(\frac{d^3}{d\xi^3} f(\xi) \right)_{\xi=+1} = 0 \quad (35)$$

Introducing the general solutions (32) and (33) into equations (34) and (35) gives the equations from which the wavenumbers λ_i and the coefficients $a_{s,i}$ and $a_{a,i}$ can be calculated. The wavenumber λ_i of a mode i is approximately given by

$$\lambda_i = \frac{\pi}{4} (1 + 2i) \quad (36)$$

This approximation is very accurate for large i . For small i the differences are only of the order of a few percent. According to equation (31) the normalised analytical singular values σ_i are the squares of the wavenumbers λ_i .

3.3 Comparison between SVD-modes and analytical modes

3.3.1 Example (a)

One can derive an expression for the singular values $\sigma_{\text{svd,an},i}$ expected from SVD based on the normalised analytical singular values σ_i . From the equations (3) and (4) one gets

$$\sigma_{\text{svd},i}^2 = \frac{\langle \mathbf{A} \mathbf{v}_i, \mathbf{A} \mathbf{v}_i \rangle}{\langle \mathbf{u}_i, \mathbf{u}_i \rangle} = \frac{\langle \mathbf{A} \mathbf{v}_i, \mathbf{A} \mathbf{v}_i \rangle}{\langle \mathbf{v}_i, \mathbf{v}_i \rangle}$$

$$\begin{aligned}
&= \frac{n_{\text{sig}}}{n_{\text{act}}} \frac{\langle \mathbf{A} \mathbf{v}_i, \mathbf{A} \mathbf{v}_i \rangle}{n_{\text{sig}}} / \frac{\langle \mathbf{v}_i, \mathbf{v}_i \rangle}{n_{\text{act}}} \\
&= \frac{n_{\text{sig}}}{n_{\text{act}}} \frac{\epsilon_{\text{sig},i}^2}{\epsilon_{\text{act},i}^2}, \tag{37}
\end{aligned}$$

where $\epsilon_{\text{sig},i}$ and $\epsilon_{\text{act},i}$ are the r.m.s. values of the signals and the actuator positions, respectively. To derive an expression for $\epsilon_{\text{sig},i}$ let d be the length of a segment, n_{seg} the number of segments, and $2D = n_{\text{seg}}d$ the length of the full linear chain. If $f_i(x)$ is one of the analytical normal modes going through the centers of the segments and the x_j are the locations of the sensors, the mean square $\epsilon_{\text{sig},i}^2$ of the signals is approximately given by

$$\epsilon_{\text{sig},i}^2 = d^2 \frac{1}{n_{\text{sig}}} \sum_{j=1}^{n_{\text{sig}}} \left(\frac{df_i(x)}{dx} \right)_{x=x_j}^2 \tag{38}$$

For a very large number of segments the averaged sum can be replaced by the integral expressions in equation (17) with $i = j$, leading to the analytical mean square $\epsilon_{\text{sig,an},i}^2$ of the signals :

$$\epsilon_{\text{sig,an},i}^2 = \frac{1}{2} \left(\frac{d}{D} \right)^2 \int_{-1}^{+1} \left(\frac{df_i(\xi)}{d\xi} \right)^2 d\xi \tag{39}$$

Dividing equation (39) by the analytical mean square $\epsilon_{\text{act,an},i}^2$ of the positions

$$\epsilon_{\text{act,an},i}^2 = \frac{1}{2} \int_{-1}^{+1} f_i^2(\xi) d\xi \tag{40}$$

and using equation (25) gives

$$\begin{aligned}
\frac{\epsilon_{\text{sig,an},i}^2}{\epsilon_{\text{act,an},i}^2} &= \left(\frac{d}{D} \right)^2 \int_{-1}^{+1} \left(\frac{df_i(\xi)}{d\xi} \right)^2 d\xi / \int_{-1}^{+1} f_i^2(\xi) d\xi \\
&= \left(\frac{d}{D} \right)^2 \sigma_i^2 = d^2 \tilde{\sigma}_i^2 \tag{41}
\end{aligned}$$

Introducing equation (41) into equation (37) and taking the square root gives an expression not any more for the true singular values $\sigma_{\text{svd},i}$ but for the ones $\sigma_{\text{svd,an},i}$ based on the analytical approximation with an infinite number of segments. The relationship between the normalised analytical singular value σ_i of the mode i and the corresponding one $\sigma_{\text{svd,an},i}$ expected from SVD is then

$$\sigma_{\text{svd,an},i} = \sqrt{\frac{n_{\text{sig}}}{n_{\text{act}}}} \frac{d}{D} \sigma_i \tag{42}$$

For a chain with 100 segments figure 3a shows the singular values $\sigma_{\text{svd,an},i}$ according to equation (42) (crosses) and the true singular values $\sigma_{\text{svd},i}$ calculated by SVD (circles). As one would expect, they only coincide for the lowest smooth modes. For the higher modes the analytical calculation overestimates the singular values. This can also be seen in figure 3b which shows the ratios of $\sigma_{\text{svd,an},i}$ to $\sigma_{\text{svd},i}$. Also for the lowest modes these ratios are not exactly equal to 1, but approximately equal to $1 + 0.5/n_{\text{seg}}$. For a large number of segments the shapes of the SVD solutions with the smallest singular values are in perfect agreement with the ones of the analytical solutions. Since the normal modes are used for the alignment of segmented mirrors, a common question is how the signal errors propagate to actuator errors, that is, which r.m.s. $\epsilon_{\text{act,n}}$ of the actuator errors is generated by noise in the signals with a given r.m.s. of $\epsilon_{\text{sig,n}}$. The r.m.s. $\epsilon_{\text{act,n}}$ can be calculated by a sum involving the n_{nz} non-zero singular values. Two r.m.s. values will be calculated. An analytical one denoted by $\epsilon_{\text{act,n,an}}$, where the sum is formed with the singular values $\sigma_{\text{svd,an},i}$, and a true one denoted by $\epsilon_{\text{act,n,svd}}$, where the sum is formed with the true singular values $\sigma_{\text{svd},i}$. In general, the mean square $\epsilon_{\text{act,an}}^2$ of the actuator errors based on analytical singular values is the sum of the mean squares $\epsilon_{\text{act,an},i}^2$ of the individual modes. Using also equation (41) one gets

$$\epsilon_{\text{act,an}}^2 = \sum_{i=1}^{n_{\text{nz}}} \epsilon_{\text{act,an},i}^2 = \sum_{i=1}^{n_{\text{nz}}} \epsilon_{\text{sig,an},i}^2 \left(\frac{D}{d} \right)^2 \frac{1}{\sigma_i^2} \tag{43}$$

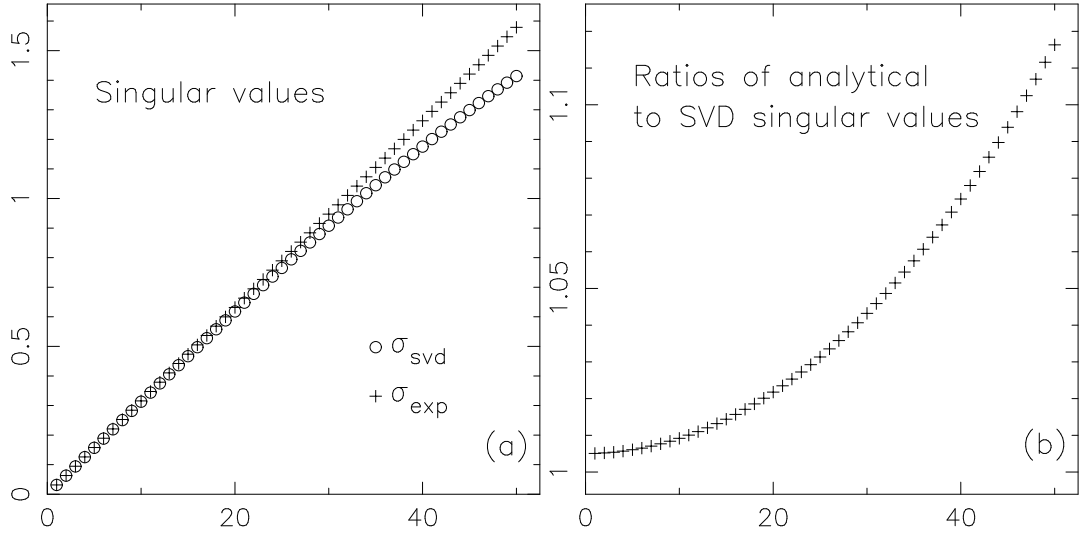


Figure 3: Example (a). **(a)** : Singular values calculated analytically (crosses) and by SVD (circles), **(b)** : Ratios of these values for the lowest 50 modes.

If the signal errors are random, each of the n_{sig} signal modes contributes an equal amount $\epsilon_{\text{sig},n,i} = \epsilon_{\text{sig},n}/\sqrt{n_{\text{sig}}}$ to the total r.m.s. $\epsilon_{\text{sig},n}$ of the signal noise. The analytically expected total mean square $\epsilon_{\text{act},n,\text{an}}^2$ of the actuator errors due to random signal noise is then, after replacing $\epsilon_{\text{sig},an,i}$ by $\epsilon_{\text{sig},n,i} = \epsilon_{\text{sig},n}/\sqrt{n_{\text{sig}}}$ and σ_i by the explicit expression in equation (24), given by

$$\epsilon_{\text{act},n,\text{an}}^2 = \epsilon_{\text{sig},n}^2 \frac{1}{\pi^2} \left(\frac{2D}{d} \right)^2 \frac{1}{n_{\text{sig}}} \sum_{i=1}^{n_{\text{nz}}} \frac{1}{i^2} \quad (44)$$

For a large number of segments n_{sig} can be replaced by $2D/d$. Furthermore, because of its fast convergence, the sum from 1 to n_{nz} is, for large n_{nz} , approximately equal to the sum from 1 to infinity, with a value of $\pi^2/6$. All this finally gives

$$\epsilon_{\text{act},n,\text{an}} \approx \epsilon_{\text{sig},n} \sqrt{\frac{1}{6}} \sqrt{\frac{2D}{d}} \quad (45)$$

For a given r.m.s. of the signal noise the r.m.s. of the actuator error therefore scales, as one would expect, with the square root of the number of segments. Equation (44) can also be written as

$$\epsilon_{\text{act},n,\text{an}}^2 = \epsilon_{\text{sig},n}^2 \frac{1}{n_{\text{act}}} \sum_{i=1}^{n_{\text{nz}}} \frac{1}{\sigma_{\text{svd},an,i}^2} \quad (46)$$

Similarly, the true r.m.s. $\epsilon_{\text{act},n,\text{svd}}$ calculated with the true SVD singular values $\sigma_{\text{svd},i}$ is given by

$$\epsilon_{\text{act},n,\text{svd}}^2 = \epsilon_{\text{sig},n}^2 \frac{1}{n_{\text{act}}} \sum_{i=1}^{n_{\text{nz}}} \frac{1}{\sigma_{\text{svd},i}^2} \quad (47)$$

The result from equation (47) is effectively identical to the one from equation (45). The same result is also obtained by simple statistical considerations, that is by summing up random piston movements along a line of segments and calculating the r.m.s. after subtracting the average.

3.3.2 Example (b)

The expression for $\sigma_{\text{svd},an,i}$ can be derived in the same way as in section 3.3.1. One gets for a specific mode i

$$\left(\frac{\epsilon_{\text{sig},an,i}}{\epsilon_{\text{act},an,i}} \right)^2 = \frac{d^2}{D^4} \int_{-1}^{+1} \left(\frac{df_i(\xi)}{d\xi} \right)^4 d\xi \bigg/ \int_{-1}^{+1} f_i^2(\xi) d\xi \quad (48)$$

$$= \frac{d^2}{D^4} \sigma_i^2 = d^2 \tilde{\sigma}_i^2 \quad (49)$$

with $\sigma_i = D^2 \tilde{\sigma}_i$. Here $\epsilon_{\text{sig,an},i}$ is the r.m.s. of the angular signal error in radians. The singular value $\sigma_{\text{svd,an},i}$ expected from SVD is then related to the corresponding analytical singular value σ_i by

$$\sigma_{\text{svd,an},i} = \sqrt{\frac{n_{\text{sig}}}{n_{\text{act}}}} \frac{d}{D^2} \sigma_i \quad (50)$$

For a chain with 100 segments figure 4a shows the square roots of the singular values $\sigma_{\text{svd,an},i}$ (crosses), that is the wavenumbers corresponding to $\sigma_{\text{svd,an},i}$ according to equation (31), and of the true ones $\sigma_{\text{svd},i}$ (circles). Figure 4a for the wavenumbers is very similar to the corresponding figure 3a for the singular values of example (a). Also the figure 4b for the ratios of the square roots of $\sigma_{\text{svd,an},i}$ to the square roots of $\sigma_{\text{svd},i}$ is effectively identical to the corresponding figure 3b of example (a) for the ratios of the singular values. The total mean

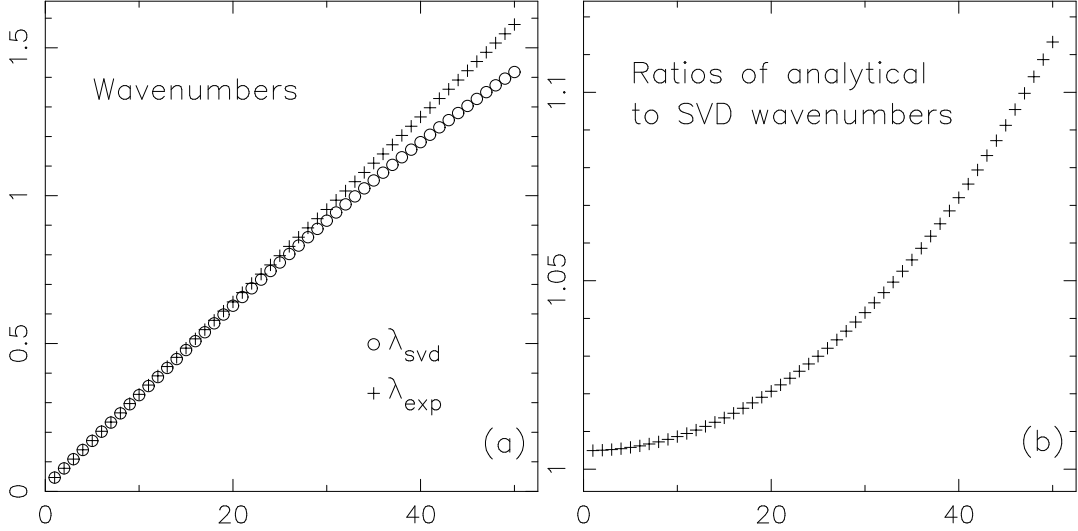


Figure 4: Example (b). **(a)** : Wavenumbers calculated analytically (crosses) and by SVD (circles), **(b)** : Ratios of these values for the lowest 50 modes.

square of the actuator errors is given by, using also equation (36) for the analytical singular values,

$$\epsilon_{\text{act,n,an}}^2 = \epsilon_{\text{sig,n}}^2 \left(\frac{4}{\pi} \right)^4 \frac{D^4}{d^2} \frac{1}{n_{\text{sig}}} \sum_{i=1}^{n_{\text{nz}}} \left(\frac{1}{1+2i} \right)^4 \quad (51)$$

Next, n_{sig} is replaced by $2D/d$. Furthermore, because of its fast convergence, the sum from 1 to n_{nz} is, for large n_{nz} , approximately equal to the sum from 1 to infinity, with a value of $\pi^4/120 - 1$. All this finally gives

$$\epsilon_{\text{act,n,an}} \approx 0.0982 D \sqrt{\frac{2D}{d}} \epsilon_{\text{sig,n}} \quad (52)$$

For a chain of 100 segments the difference between the true value $\epsilon_{\text{act,n,svd}}$ obtained from equation (47) applied to example (b) and $\epsilon_{\text{act,n,an}}$ from equation (52) is less than 1%. The solid lines in figure 2 show the analytical solutions with the three smallest singular values. Clearly, they are in perfect agreement with the SVD solutions.

4 Analytical solutions for two-dimensional segmentation

4.1 General remarks

There are several combinations of signals and actuator positions which could be studied. In this chapter we discuss mainly two examples which are of particular interest for the alignment and phasing of segmented mirrors.

We assume that the segments are hexagonal and the signals are measured at locations along the intersegment edges as shown in figure 5. In both examples the signals are the relative vertical displacements between adjacent segments at the locations of the sensors. Such signals can be obtained by optical measurements or by position sensors. In principle, the signals can also include the relative tilts between adjacent segments, defined here as

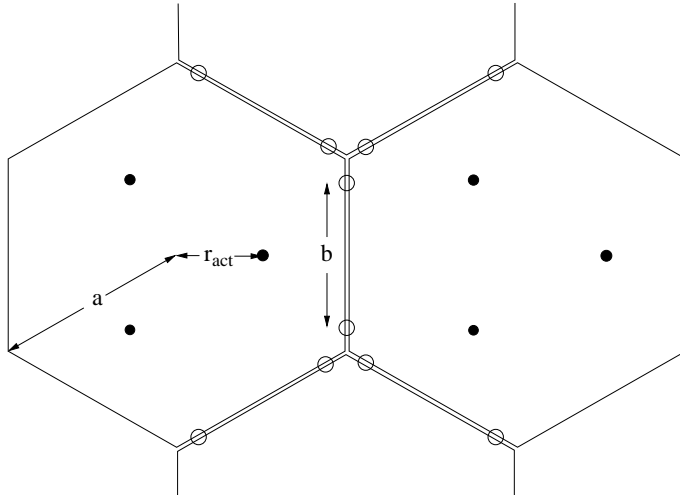


Figure 5: Locations of the sensors at the intersegment edges of hexagonal segments. The filled circles in the segments mark the positions of the actuators.

a change in the slope of the segments perpendicular to the edges at the locations of the sensors. Usually, the signals generated by relative tilts are much smaller than signals generated by relative vertical displacements [6]. Except for one particular mode, the defocus mode, which is discussed in section 5.4, relative tilts at the sensors are therefore of less significance.

The two examples differ in the number of the degrees of freedom for the movements of the segments.

- *Piston movements*

In this case, which is the two-dimensional equivalent of the one-dimensional example (a) presented in section 3.2.1, the segments can only move in piston and the positions of the three actuators of one segment are therefore all identical. The signals along one intersegment edge are all the same and it would be sufficient to consider just one signal along one edge. This example describes a situation where the segments have already been perfectly aligned in tilt and the remaining phasing errors are corrected by pure piston movements of the segments, a procedure which is used for the phasing of the segmented primary mirror of the Keck telescope based on optical measurements.

- *Piston, tip and tilt movements*

In this case, which is to some extent related to the one-dimensional example (b) presented in section 3.2.2, there are three degrees of freedom for the movements of the segments, namely piston, tip and tilt. It describes situations where a full correction of the misalignments including phasing is based on relative vertical displacement signals at the locations shown in figure 5. It is used for the fast stabilization of the alignment in the Keck telescope with signals obtained by position sensors.

The sensors at the edges of the hexagonal segments detect signals in the three directions $\theta_1 = -60^\circ$, $\theta_2 = 0^\circ$ and $\theta_3 = 60^\circ$ with respect to the horizontal axis in figure 5. The derivative of a function $f(r, \varphi)$ in one of the directions θ_k , $k = 1, 2, 3$, expressed as derivatives with respect to the radial and azimuthal coordinates r and φ of a cylindrical coordinate system, is given by

$$T_k f(r, \varphi) = \frac{\partial}{\partial s_{\theta_k}} f(r, \varphi) = \frac{1}{R} \left(\cos(\varphi - \theta_k) \frac{\partial}{\partial \rho} - \frac{\sin(\varphi - \theta_k)}{\rho} \frac{\partial}{\partial \varphi} \right) f(\rho, \varphi), \quad (53)$$

In the limit of infinitesimally small segments the lowest SVD modes always follow rotational symmetries n . They can therefore be written as a product of a radial and an azimuthal component :

$$f(r, \varphi) = f_n(r) \cos(n\varphi) \quad (54)$$

The differential operators for curvatures are second derivatives based on the operator in equation (53). Here we use the following approximation. Strictly speaking, the curvature K along a direction s is defined by

$$K = \frac{d^2 f}{ds^2} / \left[1 + \left(\frac{df}{ds} \right)^2 \right]^{3/2} \quad (55)$$

Since the derivative in the denominator is small compared to unity, we will replace the denominator by 1. This is equivalent to approximating the spherical surface by a paraboloid with a radial dependence on ρ^2 .

4.2 Piston movements

The two-dimensional case which is equivalent to the one-dimensional example in section 3.2.1 is a configuration where the segments can only perform piston movements and the sensors measure only the relative vertical displacements. In this case the differential operator is given by the operator T_k in equation (53). The starting point for the derivation of the analytical normal modes is a vector product averaged over the three directions θ_k :

$$\frac{1}{3} \sum_{k=1}^3 \langle T_k f_i(r, \varphi), T_k f_j(r, \varphi) \rangle = \frac{1}{3} \frac{1}{\pi(1-\rho_1^2)} \sum_{k=1}^3 \int d\varphi \int_{\rho_1}^1 \rho d\rho (T_k f_i(\rho, \varphi)) (T_k f_j(\rho, \varphi)) \quad (56)$$

After introducing equation (54), integrating over the azimuth angle φ , and summing over k equation (56) becomes

$$\frac{1}{3} \sum_{k=1}^3 \langle T_k f_i(r, \varphi), T_k f_j(r, \varphi) \rangle = \frac{1}{2R^2} \frac{1+\delta_{n,0}}{1-\rho_1^2} \int_{\rho_1}^1 \rho d\rho \left[\left(\frac{d}{d\rho} f_{n,i}(\rho) \right) \left(\frac{d}{d\rho} f_{n,j}(\rho) \right) + \frac{n^2}{\rho^2} f_{n,i}(\rho) f_{n,j}(\rho) \right] \quad (57)$$

Following the procedure outlined in section 2 one gets

$$L^F L = -\frac{1}{2R^2} L_{B,n} \quad (58)$$

$$\underline{\beta}_L[f_{n,i}, f_{n,j}] = \frac{1}{2R^2} \frac{1+\delta_{n,0}}{1-\rho_1^2} \left[\left(\frac{d}{d\rho} f_{n,i}(\rho) \right) f_{n,j}(\rho) \right]_{\rho_1}^1 \quad (59)$$

where $L_{B,n}$ is the operator appearing in the Bessel differential equation :

$$L_{B,n} = \frac{d^2}{d\rho^2} + \frac{1}{\rho} \frac{d}{d\rho} - \frac{n^2}{\rho^2} \quad (60)$$

The general solution of

$$L_{B,n} f_n(\rho) = -\sigma^2 f_n(\rho) \quad (61)$$

with σ related to $\tilde{\sigma}$ in equation (11) by $\sigma = \sqrt{2}R\tilde{\sigma}$ is a sum of the Bessel functions $J_n(\sigma\rho)$ and $Y_n(\sigma\rho)$ with coefficients c_J and c_Y :

$$f_n(\rho) = c_J J_n(\sigma\rho) + c_Y Y_n(\sigma\rho) \quad (62)$$

For arbitrary functions $f_{n,j}$ taken from the set of general solutions (62) the boundary functional (59) vanishes if the expression in the square brackets is zero for both $\rho = \rho_1$ and $\rho = 1$, that is if the derivatives vanish at both the inner and outer edges of the mirror. Introducing the general solution (62) into the two boundary conditions gives a set of two linear homogeneous equation in c_J and c_Y from which the infinite set of normalised analytical singular values $\sigma_{n,i}$ and the corresponding ratios $(c_Y/c_J)_{n,i}$ can be obtained. As in the corresponding

one-dimensional example discussed in section 3.2.1 the singular values $\sigma_{n,i}$ are identical to the wavenumbers of the functions, in this case two Bessel functions, contributing to the solution (62).

For the rotational symmetries 0, 1, and 2 figure 6 shows, for $\rho_1 = 0.1$, the four analytical normal modes with the smallest singular values $\sigma_{n,i}$. Like the Zernike polynomials the modes can be classified according to their rotational symmetries and, within each rotational symmetry, according to their number of nodes, that is zeros along the radial coordinate. The only mode, which is, compared with the set of Zernike modes, missing in the set $\{f_{n,i}\}$ is the lowest mode of rotational symmetry 0 with no nodes. This reflects the fact that a uniform piston movement of all segments does not generate relative vertical displacements at intersegment edges.

The major difference to the Zernike polynomials is that, due to the boundary conditions following from equation (59), the first derivatives are, as in the one-dimensional example in section 3.2.1, zero at the edges. In

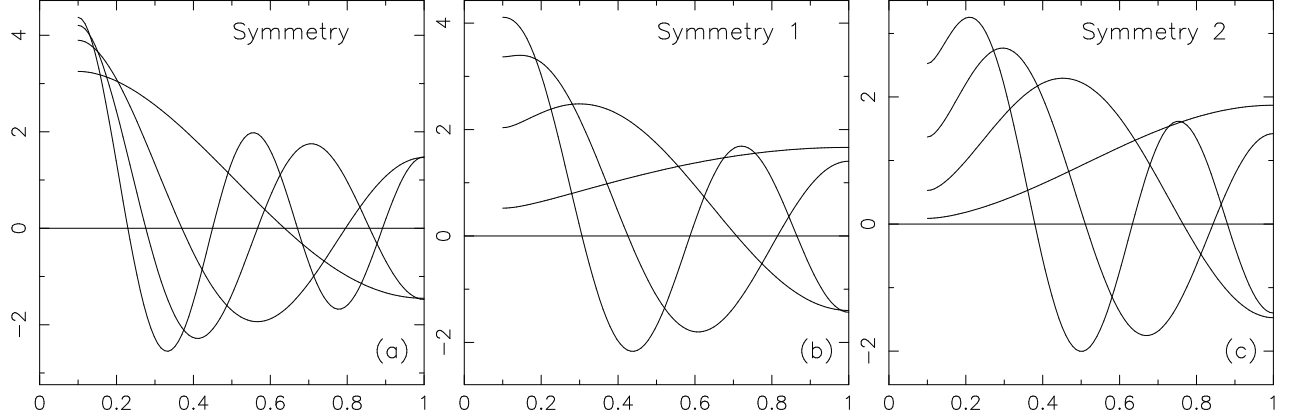


Figure 6: Lowest analytical normal modes of an annular mirror with $\rho_1 = 0.1$ for pure piston movements for the rotational symmetries 0, 1, and 2.

the case of a completely filled mirror, that is $\rho_1 = 0$, the function $Y_n(\sigma\rho)$, which diverges at $\rho = 0$, drops out of the general solution, which is then given by

$$f_n(\rho) = c_J J_n(\sigma\rho) \quad (63)$$

In this case the expression inside the square brackets of the boundary functional (59) is automatically zero for $\rho = 0$. This leaves therefore only one boundary condition which is sufficient to determine the infinite set of normalised analytical singular values $\sigma_{n,i}$ which are also identical to the wavenumbers. The functions look similar to the ones in figure 6, but now, for all symmetries $n > 0$, they are zero at the centre of the mirror.

4.3 Piston, tip and tilt movements

4.3.1 Differential operator

As in section 4.2 the sensors detect only relative vertical displacements, but the segments can now be controlled in piston, tip and tilt. Let a smooth function over hexagonal areas be approximated by planes. For a spherical surface this can be done without generating relative axial displacements. The sensors therefore measure locally only the difference to a surface with, also locally, a constant curvature in all directions. This is the same as the torsion of the surface which is given by, using also equation (54),

$$\begin{aligned} L_k f(r, \varphi) &= \frac{\partial^2 f(r, \varphi)}{\partial s_{\theta_k} \partial s_{\theta_k - 90^\circ}} \\ &= \frac{1}{2R^2} [\sin(2(\varphi - \theta_k)) \cos(n\varphi) L_{n,1} f_n(\rho) + 2 \cos(2(\varphi - \theta_k)) \sin(n\varphi) L_{n,2} f_n(\rho)] \end{aligned} \quad (64)$$

with the two operators $L_{n,1}$ and $L_{n,2}$ defined by

$$L_{n,1} = \frac{d^2}{d\rho^2} - \frac{1}{\rho} \frac{d}{d\rho} + \frac{n^2}{\rho^2} \quad (65)$$

$$L_{n,2} = -\frac{n}{\rho} \frac{d}{d\rho} + \frac{n}{\rho^2} \quad (66)$$

4.3.2 Derivation of the analytical normal modes

The procedure outlined in section 2 starts off with the following vector product averaged over the three direction Θ_k :

$$\frac{1}{3} \sum_{k=1}^3 \langle L_k f_i(r, \varphi), L_k f_j(r, \varphi) \rangle = \frac{1}{3} \frac{1}{\pi(1-\rho_1^2)} \sum_{k=1}^3 \int d\varphi \int_{\rho_1}^1 \rho d\rho (L_k f_i(\rho, \varphi)) (L_k f_j(\rho, \varphi)) \quad (67)$$

After introducing equation (54), integrating over the azimuth angle φ , and summing over the three directions denoted by k one gets

$$\begin{aligned} \frac{1}{3} \sum_{k=1}^3 \langle L_k f_i(r, \varphi), L_k f_j(r, \varphi) \rangle &= \frac{1}{8R^4} \frac{1+\delta_{n,0}}{1-\rho_1^2} \int_{\rho_1}^1 \rho d\rho [(L_{n,1} f_{n,i}(\rho))(L_{n,1} f_{n,j}(\rho)) + \\ &\quad 4(L_{n,2} f_{n,i}(\rho))(L_{n,2} f_{n,j}(\rho))] \end{aligned} \quad (68)$$

A straightforward calculation shows that

$$L^F L = \frac{1}{8R^4} L_{B,n}^2 \quad (69)$$

The boundary functional is given by

$$\begin{aligned} \underline{\beta}_L[f_{n,i} f_{n,j}] &= \frac{1}{8R^4} \frac{1+\delta_{n,0}}{1-\rho_1^2} \left\{ \left[\left(\rho \frac{d^2}{d\rho^2} f_{n,i}(\rho) - \frac{d}{d\rho} f_{n,i}(\rho) + \frac{n^2}{\rho} f_{n,i}(\rho) \right) \frac{d}{d\rho} f_{n,j}(\rho) \right]_{\rho_1}^1 + \right. \\ &\quad \left. \left[\left(-\rho \frac{d^3}{d\rho^3} f_{n,i}(\rho) - \frac{d^2}{d\rho^2} f_{n,i}(\rho) + (1+3n^2) \frac{1}{\rho} \frac{d}{d\rho} f_{n,i}(\rho) - 4 \frac{n^2}{\rho^2} f_{n,i}(\rho) \right) f_{n,j}(\rho) \right]_{\rho_1}^1 \right\} \end{aligned} \quad (70)$$

With σ related to $\tilde{\sigma}$ in equation (11) by $\sigma = \sqrt{8}R^2\tilde{\sigma}$ the fourth-order differential operator appearing in

$$L_{B,n}^2 f_n(\rho) = \sigma^2 f_n(\rho) \quad (71)$$

can be written as a product of two second-order differential operators. Equation (71) then becomes

$$(L_{B,n} + \sigma)(L_{B,n} - \sigma)f_n(\rho) = 0 \quad (72)$$

With the same definition (31) of λ as in section 3.2.2 the general solution of (72) is a sum of the Bessel functions $J_n(\lambda\rho)$, $Y_n(\lambda\rho)$, $I_n(\lambda\rho)$, and $K_n(\lambda\rho)$ with coefficients c_J , c_Y , c_I and c_K :

$$f(\rho) = c_J J_n(\lambda\rho) + c_Y Y_n(\lambda\rho) + c_I I_n(\lambda\rho) + c_K K_n(\lambda\rho) \quad (73)$$

For an arbitrary choice of the functions $f_{n,j}$ the boundary functional (70) is zero if the expressions in both square brackets vanish for $\rho = \rho_1$ and $\rho = 1$. Introducing (73) into the four boundary conditions gives a system of four linear homogeneous equations in c_J , c_Y , c_I , and c_K from which the infinite set of normalised wavenumbers $\lambda_{n,i}$ and the corresponding ratios of c_Y , c_I , and c_K to c_J can be obtained. Similarly to the corresponding one-dimensional example the singular values $\sigma_{n,i}$ are the squares of the wavenumbers $\lambda_{n,i}$.

For the rotational symmetries 0, 1, and 2 and $\rho_1 = 0.1$ figure 7 shows the four analytical normal modes with the lowest singular values $\sigma_{n,i}$. Using the classification of the modes introduced in section 4.2 three modes are missing compared with the set of Zernike modes. Two of them are the two lowest modes of rotational symmetry 0 without and with one node, corresponding to Zernike piston and defocus, and the third one is the lowest

mode of rotational symmetry 1 corresponding to Zernike tilt. All three modes can be generated without relative vertical displacements at intersegment edges.

The functions are somewhat similar to the corresponding Zernike polynomials, but should better be compared with the elastic minimum energy modes of circular plates (see section 7). For the case of a full mirror, that is

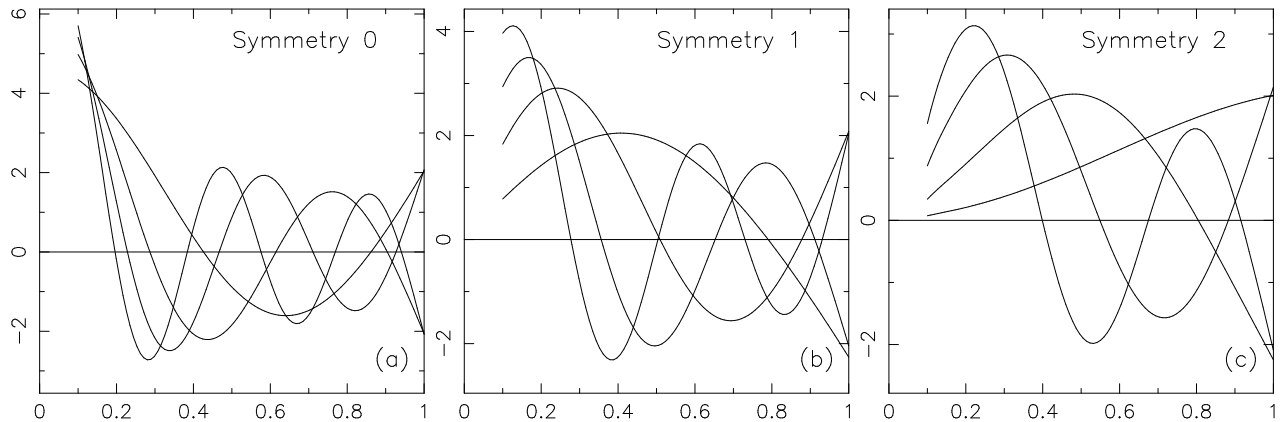


Figure 7: Lowest analytical normal modes of an annular mirror with $\rho_1 = 0.1$ for piston, tip and tilt movements for the rotational symmetries 0, 1, and 2.

$\rho_1 = 0$, the Bessel functions $Y_n(\lambda\rho)$ and $K_n(\lambda\rho)$, which diverge at $\rho = 0$, drop out of the general solution, which is then given by

$$f = c_J J_n(\lambda\rho) + c_I I_n(\lambda\rho) \quad (74)$$

The expressions in the two square brackets of the boundary functional (70) are automatically zero for $\rho = 0$. This leaves two boundary conditions which are sufficient to calculate the wavenumbers $\lambda_{n,i}$ and the corresponding ratios $(c_I/c_J)_{n,i}$. The functions look similar to the ones in figure 7, but now, for all symmetries $n > 0$, they are zero at the centre of the mirror.

5 Comparison with SVD results

5.1 SVD programs

All SVD calculations were done with computer programs supplied by G. Chanan [5]. They were developed for and applied to the control of the segmented primary mirror of the Keck telescope. Most of the data used in this paper were obtained for the segmented mirror shown in figure 8. In the following, the radius of the segments is, as shown in figure 5, denoted by a and the distance between the sensors along one intersegment edge by b . For the numerical SVD-calculations we used the parameters $a = 0.5$ m, $b = 0.3078$ m, and $R = 15.05$ m. The segments in figure 8 are the ones with the centres inside the range of normalised radii ρ of $0.30 < \rho < 1.0$. This mirror has got 1002 segments and 5688 sensors. The radius of the circle r_{act} defined by the actuator locations shown in figure 5 was $r_{\text{act}} = 0.52275 a$. Calculations were also done for a geometry similar to the one shown in figure 8, but without a central hole. This mirror has got 1099 segments and 6348 sensors.

5.2 Piston movements

5.2.1 Mode shapes

The number of SVD modes with non-zero singular values is $n_{\text{nz}} = n_{\text{seg}} - 1$. One mode with a singular value equal to zero, which corresponds to the missing analytical mode in section 4.2, is related to a uniform piston

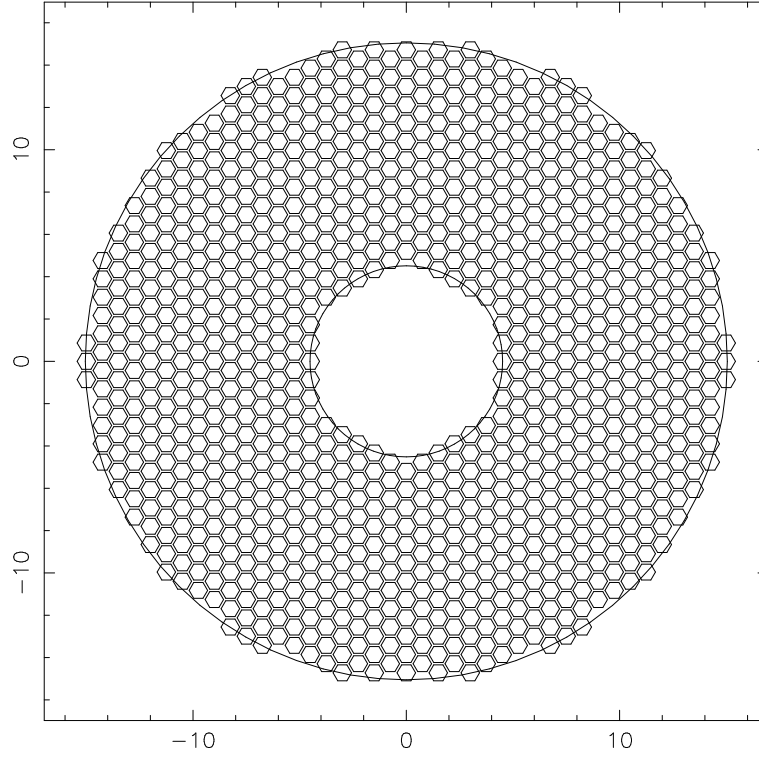


Figure 8: Segmentation used for the SVD calculations.

movement of all segments. For a few low order modes figure 9 shows the traces along a diameter for a full and an annular mirror. Especially for the full mirror the agreement between the shapes of the normal modes obtained with SVD (circles) and analytically (solid lines) in section 4.2 is excellent. The deviations close to the inner hole of the annular mirror are to be expected since this edge is less accurately defined because of the smaller number of segments.

5.2.2 Singular values

For pure piston movements a sensor signal is proportional to the difference between the values of an analytical normal mode $f_{n,i}$ at adjacent segment centres. To the first approximation, this is proportional to the slopes of $f_{n,i}$ midway between two centres along the line connecting the two centres times the distance $\sqrt{3}a$ between the two centres. The mean square $\epsilon_{\text{sig},n,i}^2$ of the sensor signals of the mode (n,i) is therefore

$$\epsilon_{\text{sig},n,i}^2 = \left(\sqrt{3}a\right)^2 \frac{1}{n_{\text{sig}}} \sum_{j=1}^{n_{\text{sig}}} T_{n,i,j}^2, \quad (75)$$

where $T_{n,i,j}$ is the slope of the mode i of rotational symmetry n perpendicular to the edge at the location of the sensor j . For a very large number of segments the averaged sum in equation (75) can be replaced by the integral expressions in equation (57) with $i = j$:

$$\epsilon_{\text{sig},\text{an},n,i}^2 = \frac{3a^2}{2R^2} \frac{1 + \delta_{n,0}}{1 - \rho_1^2} \int_{\rho_1}^1 \rho \, d\rho \left[\left(\frac{d}{d\rho} f_{n,i}(\rho) \right)^2 + \frac{n^2}{\rho^2} f_{n,i}^2(\rho) \right] \quad (76)$$

After dividing by the mean square $\epsilon_{\text{act},\text{an},n,i}^2$ of the actuator positions

$$\epsilon_{\text{act},n,i}^2 = \frac{1 + \delta_{n,0}}{1 - \rho_1^2} \int_{\rho_1}^1 \rho \, d\rho f_{n,i}^2(\rho) \quad (77)$$

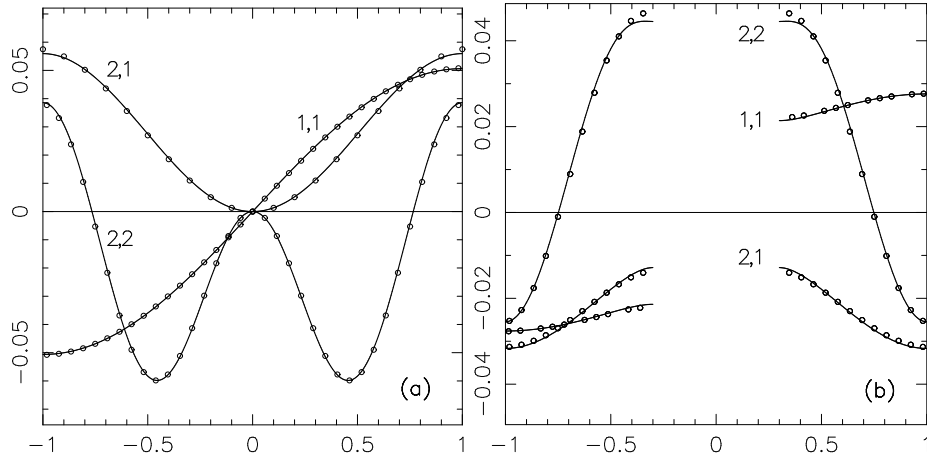


Figure 9: Normal modes calculated by SVD (circles) and analytical normal modes (solid lines) for pure piston movements. The first index along a curve denotes the rotational symmetry and the second one the order within the symmetry. **(a)** : Full mirror, **(b)** : Annular mirror with $\rho_1 = 0.3$.

one gets

$$\frac{\epsilon_{\text{sig,an},n,i}^2}{\epsilon_{\text{act,an},n,i}^2} = \frac{3a^2}{2R^2} \sigma_{n,i}^2 = 3a^2 \tilde{\sigma}_{n,i}^2 \quad (78)$$

where $\sigma_{n,i} = \sqrt{2}R\tilde{\sigma}_{n,i}$ are the normalised analytical singular values. Similarly to section 3.3.1 one finally gets for the relationship between a singular value $\sigma_{\text{svd,an},n,i}$ expected analytically from SVD and the corresponding $\sigma_{n,i}$

$$\sigma_{\text{svd,an},n,i} = \sqrt{\frac{3}{2} \frac{n_{\text{sig}}}{n_{\text{act}}}} \frac{a}{R} \sigma_{n,i} \quad (79)$$

Since the ratio $n_{\text{sig}}/n_{\text{act}}$ is effectively constant for highly segmented mirrors, the singular values for a specific mode (n,i) expected from SVD scale with a/R . Figure 10a shows for the lowest 25 normal modes the true singular values $\sigma_{\text{svd},n,i}$ given by SVD (circles) on the one hand and the ones $\sigma_{\text{svd,an},n,i}$ (crosses) according to equation (79) on the other hand. The agreement is quite satisfactory. Figure 10b, displaying the ratios of $\sigma_{\text{svd,an},n,i}$ to $\sigma_{\text{svd},n,i}$, shows that for the higher modes the analytical calculation overestimates the singular values.

5.2.3 Error propagation

Starting from equation (78) one can derive how the total r.m.s. $\epsilon_{\text{act,n,an}}$ of the actuator errors generated by a given r.m.s. $\epsilon_{\text{sig,n}}$ of the signal errors scales with the number of segments. The procedure is the same as the one used in section 3.3.1. One gets

$$\epsilon_{\text{act,n,an}}^2 = \epsilon_{\text{sig,n}}^2 \frac{2R^2}{3a^2} \frac{1}{n_{\text{sig}}} \sum_{n,i} \frac{1}{\sigma_{n,i}^2}, \quad (80)$$

where the sum runs over the $n_{\text{nz}} = n_{\text{seg}} - 1$ non-zero analytical singular values. For a large number of segments the total number of segments is approximately given by

$$n_{\text{seg}} \approx \frac{2\pi}{3\sqrt{3}} \left(\frac{R}{a} \right)^2 \quad (81)$$

Neglecting the missing sensors at the edge of the mirror, the number of sensors is approximately given by

$$n_{\text{sig}} \approx 6 n_{\text{seg}} \quad (82)$$

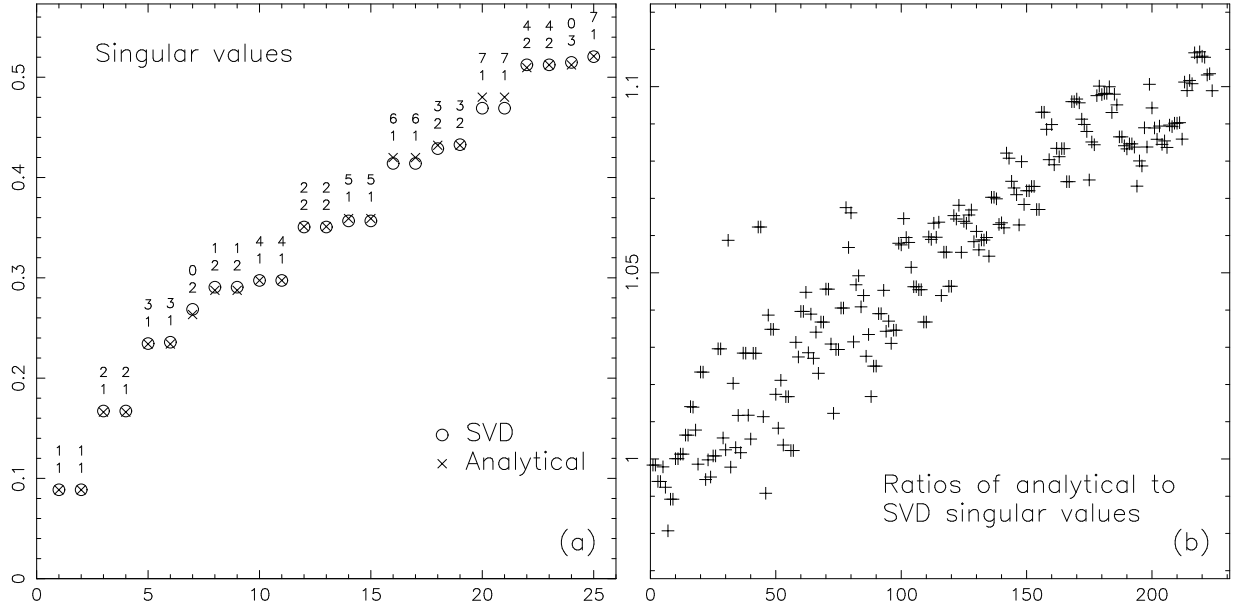


Figure 10: Singular values calculated by SVD (circles) and analytically (crosses) for pure piston movements. **(a)** : Lowest 25 modes, **(b)** : Ratios of analytically expected singular values to the ones calculated by SVD for the lowest 230 modes.

Introducing all this into equation (80) one gets

$$\epsilon_{\text{act},n,\text{an}}^2 \approx \epsilon_{\text{sig},n}^2 \frac{1}{2\pi\sqrt{3}} \sum_{n,i} \frac{1}{\sigma_{n,i}^2} \quad (83)$$

For the higher modes the analytical singular values increase approximately linearly both with the symmetry n and the order i , in the latter case, as one should expect, in steps of π . With such linear dependencies on n and i the sum in equation (83) does not converge if the number of segments goes to infinity. But it increases only very slowly, namely approximately linearly with the logarithm of n_{nz} . Therefore, $\epsilon_{\text{act},n,\text{an}}$ scales approximately with $\log(R/a)$.

For the full mirror described in section 5.1 the sum in equation (83) is approximately equal to 2.4. This gives for the r.m.s. $\epsilon_{\text{act},n,\text{an}}$ of the actuator errors

$$\epsilon_{\text{act},n,\text{an}} \approx 0.470 \epsilon_{\text{sig},n} \quad (84)$$

This is in good agreement with the true r.m.s. $\epsilon_{\text{act},n,\text{svd}} = 0.504 \epsilon_{\text{sig},n}$ of the actuator errors calculated with the true singular values $\sigma_{\text{svd},n,i}$. Similar values for $\epsilon_{\text{act},n,\text{svd}}$ are given in table 4 of reference [6]. The true value $\epsilon_{\text{act},n,\text{svd}}$ is slightly larger than $\epsilon_{\text{act},n,\text{an}}$ since, first, the singular values $\sigma_{\text{svd},\text{an},n,i}$ are larger than the true ones $\sigma_{\text{svd},n,i}$ and, second, the number of signals is smaller than the value of $6 n_{\text{seg}}$ used in the derivation of equation (84).

5.3 Piston, tip and tilt movements

5.3.1 Mode shapes

The number of non-zero singular values is $n_{\text{nz}} = n_{\text{act}} - 4$. Four normal modes calculated by SVD with singular values zero are the piston mode, the defocus mode and the two tilt modes. They correspond to the three missing analytical normal modes in section 4.3.2. Figure 11 shows for a few of the lowest modes the SVD solutions (circles) and the corresponding analytical solutions (solid lines) for a full and an annular mirror. Especially for the full mirror the agreement is excellent.

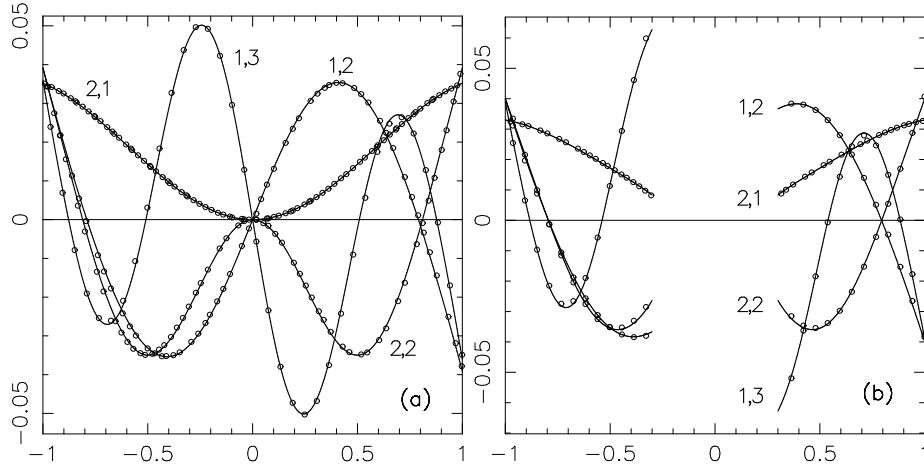


Figure 11: Normal modes calculated by SVD (circles) and analytical normal modes (solid lines) for piston, tip and tilt movements for the lowest two modes of the rotational symmetries 1 and 2. **(a)** : Full mirror, **(b)** : Annular mirror with $\rho_1 = 0.3$.

5.3.2 Singular values

The sensor signals are proportional to the difference in the slope of an analytical normal mode $f_{n,i}$ between adjacent segment centres. If only the torsion contributes to a sensor signal one has to take the slope perpendicular to the line connecting the two centres. The difference in the slope is then, to the first approximation, proportional to the torsion of $f_{n,i}$ at the location midway between the two centres, the distance $\sqrt{3}a$ between the two centres, and the distance from the midway point to the sensor, that is $b/2$. The mean square $\epsilon_{\text{sig},n,i}^2$ of the sensor signals for the mode (n, i) is therefore

$$\epsilon_{\text{sig},n,i}^2 = \left(\frac{\sqrt{3}ab}{2} \right)^2 \frac{1}{n_{\text{sig}}} \sum_{j=1}^{n_{\text{sig}}} T_{n,i,j}^2, \quad (85)$$

where $T_{n,i,j}$ is the torsion of the mode (n, i) at the location of the sensor j . For a very large number of segments the averaged sum in equation (85) can be replaced by the integral expressions in equation (68) with $i = j$:

$$\epsilon_{\text{sig,an},n,i}^2 = \frac{3a^2b^2}{32R^4} \frac{1 + \delta_{n,0}}{1 - \rho_1^2} \int_0^1 \rho d\rho [(L_{n,1}f_{n,i}(\rho))^2 + 4(L_{n,2}f_{n,i}(\rho))^2] \quad (86)$$

After dividing, as in section 5.2.2, by the mean square of the actuator positions, the ratio of the mean square of the sensors signals to the mean square of the actuator positions for a given mode (n, i) becomes

$$\frac{\epsilon_{\text{sig,an},n,i}^2}{\epsilon_{\text{act,an},n,i}^2} = \frac{3a^2b^2}{32R^4} \sigma_{n,i}^2 = \frac{3a^2b^2}{4} \tilde{\sigma}_{n,i}^2, \quad (87)$$

where $\sigma_{n,i} = \sqrt{8}R^2\tilde{\sigma}_{n,i}$ are the normalised analytical singular values. Similarly to section 3.2.1 one finally gets for the relationship between the singular value $\sigma_{\text{svd,an},n,i}$ of the mode (n, i) expected analytically from SVD and the corresponding normalised analytical one $\sigma_{n,i}$

$$\sigma_{\text{svd,an},n,i} = \sqrt{\frac{3}{32} \frac{n_{\text{sig}}}{n_{\text{act}}}} \frac{ab}{R^2} \sigma_{n,i} \quad (88)$$

Since the ratio $n_{\text{sig}}/n_{\text{act}}$ is effectively constant for highly segmented mirrors, the singular values expected from SVD scale with ab/R^2 . Figure 12a shows for the lowest 25 normal modes the true singular values $\sigma_{\text{svd},n,i}$ given by SVD (circles) on the one hand and the ones $\sigma_{\text{svd,an},n,i}$ (crosses) according to equation (88) on the other hand. The agreement is quite satisfactory. Figure 12b, displaying the ratios of $\sigma_{\text{svd,an},n,i}$ to $\sigma_{\text{svd},n,i}$, shows that for the higher modes the analytical calculation underestimates the singular values.

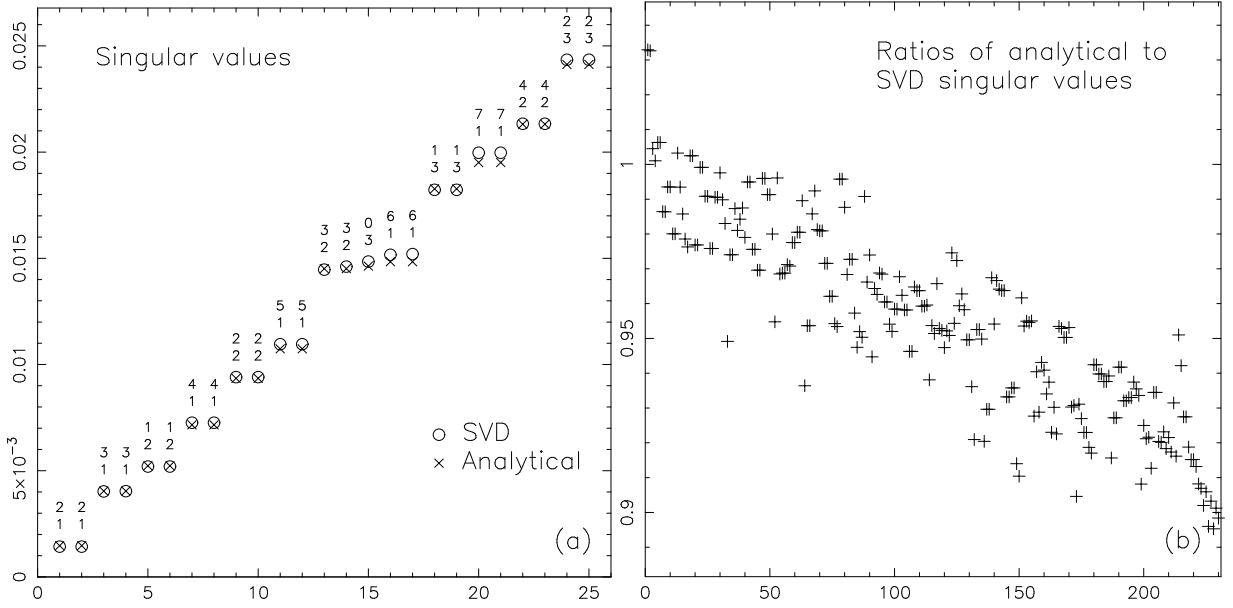


Figure 12: Singular values calculated with SVD (circles) and analytically (crosses) for piston, tip and tilt movements. (a) : Lowest 25 modes, (b) : Ratios of expected singular values to the ones calculated by SVD for the lowest 230 modes.

5.3.3 Error propagation

Starting from equation (87) one can derive an expression for the total r.m.s. $\epsilon_{\text{act},n,\text{an}}$ of the actuator errors based on the analytical singular values. The procedure is again the same as the one used in section 3.3.1. One gets

$$\epsilon_{\text{act},n,\text{an}}^2 = \epsilon_{\text{sig},n}^2 \frac{32R^4}{3a^2b^2} \frac{1}{n_{\text{sig}}} \sum_{n,i} \frac{1}{\sigma_{n,i}^2}, \quad (89)$$

where the sum runs over the $n_{\text{nz}} = n_{\text{act}} - 4$ non-zero analytical singular values. For the higher modes the square roots of the analytical singular values increase approximately linearly both with the symmetry n and the order i , in the latter case, as one should expect, in steps of π . The sum in equation (89) converges rapidly for a large number of segments. For the full mirror described in section 5.1 the limit value is approximately 0.065. Introducing this and the approximate expressions (81) and (82) into equation (89) one finally gets for the r.m.s. of the actuator errors

$$\epsilon_{\text{act},n,\text{an}} \approx 0.31 \frac{R}{b} \epsilon_{\text{sig},n} \quad (90)$$

The true r.m.s. $\sigma_{\text{act},n,\text{svd}}$ of the actuator errors is effectively the same as the one calculated from equation (90). For the currently envisaged extremely large telescopes the ratio R/b is approximately equal to 50. The r.m.s. of the actuator errors is then approximately fifteen times larger than the r.m.s. of the signal errors. This is in good agreement with the results of SVD calculations for a thirty meter telescope given in table 1 of reference [6].

5.4 Piston, tip and tilt generated by relative tilt signals

Some sensors detect in addition to the relative vertical displacements also the relative tilts between adjacent segments. One could use the same formalism as in the other examples to derive the differential equations and the boundary conditions. Unfortunately, the fourth-order differential operator cannot easily be factorised into two second-order differential operators as it could be done in equations (71) and (72). But usually the signals due to the relative tilts perpendicular to the edges are much smaller than the signals due to relative vertical displacements [6]. Most modes will then hardly be affected by the tilt signals. There is only one additional

mode of rotational symmetry zero with a non-zero singular value which converges, in the limit of the signals due to relative tilts going to zero, to the pure defocus mode with a singular value equal to zero. For small, but still non-zero tilt signals the singular value of this mode can be estimated. It is related to the integral of the mean curvature over the mirror for a mode shape proportional to pure defocus. The operator which measures the curvature along a direction θ_k is given by

$$L_k f(r, \varphi) = \frac{\partial^2 f(r, \varphi)}{\partial^2 s_{\theta_k}} = \frac{1}{R^2} \left\{ \cos(n\varphi) \left[\cos^2(\theta_k) \frac{\partial^2 f_n(\rho)}{\partial \rho^2} + \sin^2(\theta_k) \frac{1}{\rho} \left(\frac{\partial f_n(\rho)}{\partial \rho} - \frac{n^2}{\rho} f_n(\rho) \right) \right] \right. \\ \left. + \sin(n\varphi) \sin(2\theta_k) n \left(\frac{\partial f_n(\rho)}{\partial \rho} - \frac{1}{\rho} f_n(\rho) \right) \right\} \quad (91)$$

One then obtains, after introducing equation (54), integrating over the azimuth angle φ , and averaging over the three directions denoted by k , for the special case of rotational symmetry 0 and a full mirror

$$\frac{1}{3} \sum_{k=1}^3 \langle L_k f_i(r, \varphi), L_k f_i(r, \varphi) \rangle = \frac{1}{4R^4} \int_0^1 \rho d\rho \left[3 \left(\frac{d^2 f_{0,i}(\rho)}{d\rho^2} \right)^2 + \frac{3}{\rho^2} \left(\frac{df_{0,i}(\rho)}{d\rho} \right)^2 + \frac{2}{\rho} \frac{d^2 f_{0,i}(\rho)}{d\rho^2} \frac{df_{0,i}(\rho)}{d\rho} \right] \quad (92)$$

If one assumes that the lowest mode $f_{0,2}$ ($f_{0,1}$ would denote the piston mode) is equal to pure Zernike defocus $c\sqrt{3}(2\rho^2 - 1)$, where c is the r.m.s. of this mode, one gets

$$\frac{1}{3} \sum_{k=1}^3 \langle L_k f_{0,2}(r, \varphi), L_k f_{0,2}(r, \varphi) \rangle = c^2 \frac{48}{R^4} \quad (93)$$

The sensor signal is proportional to the difference in tilt between adjacent segment centres. If only the curvature contributes to the sensor signal one has to take the tilt component parallel to the line connecting the two centres. The difference in tilt is then, to the first approximation, proportional to the curvature at the location midway between the two centres, the distance $\sqrt{3}a$ between the centres and the lever g which converts the angular difference into a differential displacement [6]. The mean square $\epsilon_{\text{sig},0,2}^2$ of the sensor signals is therefore

$$\epsilon_{\text{sig},0,2}^2 = (\sqrt{3}ag)^2 \frac{1}{n_{\text{sig}}} \sum_{j=1}^{n_{\text{sig}}} T_{0,2,j}^2, \quad (94)$$

where $T_{0,2,j}$ is the curvature of the defocus mode at the location of the sensor j . In the limit of small segments the averaged sum in equation (94) can be replaced by the integral expression in equation (93) :

$$\epsilon_{\text{sig},\text{an},0,2}^2 = 144 c^2 \left(\frac{ag}{R^2} \right)^2 \quad (95)$$

After dividing, as in section 5.2.2, by the mean square c^2 of the position function, the ratio of the r.m.s. of the sensor signals to the r.m.s. of the actuator positions for the defocus mode becomes

$$\frac{\epsilon_{\text{sig},\text{an},0,2}}{\epsilon_{\text{act},\text{an},0,2}} = 12 \frac{ag}{R^2} \quad (96)$$

The singular value expected from SVD is then finally given by

$$\sigma_{\text{svd},\text{an},0,2} = 12 \sqrt{\frac{n_{\text{sig}}}{n_{\text{act}}}} \frac{ag}{R^2} \quad (97)$$

For the full mirror described in section 5.1 with $g = 23.53$ mm one gets from equation (97) $\sigma_{\text{svd},\text{an},0,2} = 0.0007206$. This is in good agreement with the result of $\sigma_{\text{svd},0,2} = 0.0007064$ obtained from a SVD calculation.

6 Relationship to modes minimizing the signals measured by the sensors

For arbitrary position functions the mean square \mathcal{J} of the signals is given $f(\xi)$ by

$$\mathcal{J} = \frac{1}{2D} \int (Lf(\xi))^2 d\xi \quad (98)$$

for the two one-dimensional examples with the operators L defined in equations (16) and (26), and for arbitrary position functions $f_n(\rho)$ by

$$\mathcal{J} = \frac{1}{2R^2} \frac{1 + \delta_{n,0}}{1 - \rho_1^2} \int_{\rho_1}^1 \rho \, d\rho \left(\left(\frac{d}{d\rho} f_n(\rho) \right)^2 + \frac{n^2}{\rho^2} f_n^2(\rho) \right) \quad (99)$$

$$\mathcal{J} = \frac{1}{8R^4} \frac{1 + \delta_{n,0}}{1 - \rho_1^2} \int_{\rho_1}^1 \rho \, d\rho \left((L_{\rho,1} f_n(\rho))^2 + 4(L_{\rho,2} f_n(\rho))^2 \right) \quad (100)$$

for the two-dimensional examples in sections 4.2 and 4.3. On the assumption that the mean square \mathcal{C} of the position functions, defined by

$$\mathcal{C} = \frac{1}{2} \int_{-1}^{+1} f^2(\xi) \, d\xi \quad (101)$$

$$\mathcal{C} = \frac{1 + \delta_{n,0}}{1 - \rho_1^2} \int_{\rho_1}^1 \rho \, d\rho f_n^2(\rho) \quad (102)$$

for the one- and two-dimensional cases, is constant, the modes which minimise the r.m.s. of the signals can be calculated by variational methods. Denoting the variation by δ one has to solve

$$\delta(\mathcal{J} - \zeta \mathcal{C}) = 0 \quad (103)$$

where ζ is a free parameter which can be interpreted the energy per unit of the r.m.s. of \mathcal{C} . This gives, with $m = 0$ and $\eta = \xi$ for the one-dimensional and $m = 1$, $\eta = \rho$, and $f = f_n$ for the two-dimensional examples

$$\frac{\delta J}{\delta f} - 2\zeta \eta^m f = 0 \quad (104)$$

or explicitly, with a prime denoting a partial derivative with respect to η ,

$$\frac{\partial J}{\partial f} - \frac{\partial}{\partial \eta} \frac{\partial J}{\partial f'} + \frac{\partial^2}{\partial \eta^2} \frac{\partial J}{\partial f''} - 2\zeta \eta^m f = 0 \quad (105)$$

For all examples given in this paper the differential equations derived from equation (105) are identical to the ones derived with the method outlined in section 2. The analytical normal modes can therefore be regarded as a special class of the modes which minimise the r.m.s. of the signals for a specified r.m.s. of the position function f . Their special characteristic is that the position modes and corresponding signal modes form orthogonal sets, which defines the boundary conditions.

7 Relationship of analytical normal modes to elastic modes

7.1 Reasons for a comparison

In future extremely large telescopes segmented mirrors will be used together with large flexible meniscus mirrors. Whereas the aberrations of the segmented mirrors are best described by the analytical normal modes derived in this paper, the deformations of the thin meniscus mirrors are best described by minimum elastic energy modes [3]. For the two examples in sects. 3.2.2 and 4.3 both types of modes are closely related and, as will be shown in this section, often very similar. This offers the possibility to correct aberrations, which are generated by segmented mirrors, by thin meniscus mirrors and vice versa.

7.2 One-dimensional segmentation

The differential equation (30) for example (b) in section 3.2.2 is identical to the one for minimum elastic energy modes of a bar. Since the boundary conditions (34) and (35) are also the same as the boundary conditions for a bar which is free at both ends, the analytical normal modes of example (b) are identical to the elastic modes of a free bar.

Table 1: Residual r.m.s. after fitting a set of elastic modes of rotational symmetry 2 to the four lowest analytical normal modes of rotational symmetry 2.

		Fitted elastic modes				
		1	2	3	4	5
Normal modes	1	0.0817	0.0238	0.0104	0.0056	0.0023
	2	0.9969	0.0053	0.0007	0.0007	0.0006
	3	0.9998	0.9998	0.0124	0.0066	0.0042
	4	1.0000	1.0000	0.9999	0.0156	0.0081

7.3 Two-dimensional segmentation

It is shown in appendix A that the orthogonal set of minimum elastic energy modes of a thin circular plate can be derived with a slightly more general method than the one introduced in section 2. For the set of elastic modes the corresponding set of curvature tensors has to be orthogonal to the corresponding set of moment tensors. This leads to the same differential equation (72) as for the case of piston, tip and tilt movements in section 4.3.2. Any differences in the shapes must then be related to the boundary conditions. For higher order modes with large wavenumbers the terms with highest derivatives in the boundary conditions dominate the other terms. If only the terms with the highest derivatives are retained, the boundary conditions for the analytical normal modes in equation (70) and the elastic modes in equations (117) and (118) below of a free plate are identical :

$$\left(\frac{d^2}{d\rho^2} f_i(\rho) \right)_{\rho=1} = 0 \quad (106)$$

$$\left(\frac{d^3}{d\rho^3} f_i(\rho) \right)_{\rho=1} = 0 \quad (107)$$

Therefore, within each rotational symmetry, the higher analytical normal modes should be very similar to the corresponding elastic modes of a circular plate. This similarity is obvious from figure 13 which compares the shapes of the lowest analytical normal modes of the rotational symmetries 0 and 2 with the shapes of the corresponding elastic modes.

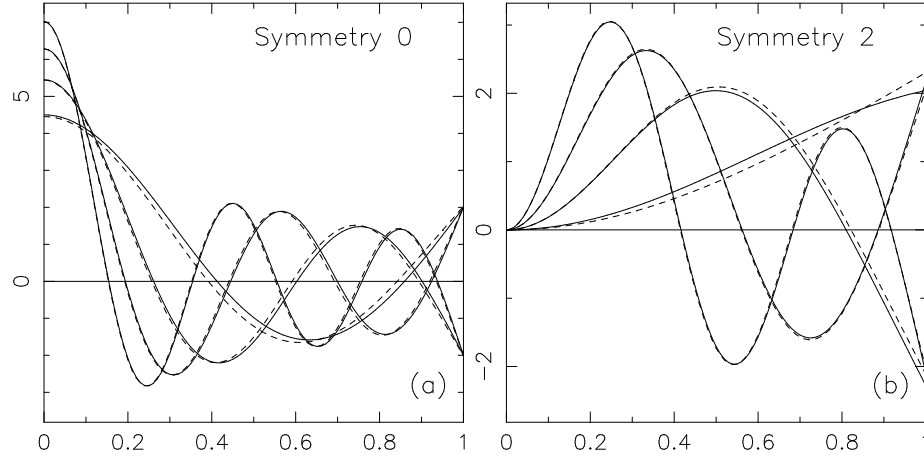


Figure 13: Comparison of the lowest analytical normal modes (solid lines) and corresponding elastic modes (dashed lines) for the rotational symmetries 0 and 2.

Table 1 shows, for an initial r.m.s. of an analytical normal mode of 1, the residual r.m.s. after fitting a given number of the lowest elastic modes of a full circular plate to the lowest four analytical normal modes of rotational symmetry 2 of a full mirror. The difference between the lowest analytical normal mode and the corresponding

lowest elastic mode is of the order of 8% and one needs to fit the lowest three elastic modes to push the residual r.m.s. to a level of 1%. The similarity of the higher order modes is expressed by the fact that the residual r.m.s. is effectively equal to 1 if the lowest $i - 1$ elastic modes are fitted to i -th analytical normal mode, but drops sharply to approximately 1% after the i -th elastic mode is included in the fit.

It is interesting to compare the probabilities of the occurrence of normal modes in a segmented mirror on the one hand with the probabilities of the occurrence of elastic modes in a monolithic mirror on the other hand. One has to choose the normal modes obtained from the more general case of piston, tip and tilt movements presented in section 4.3 because of their similarity to the elastic minimum energy modes.

The source for wavefront errors in the form of normal modes are the signals at intersegment edges. For white noise the r.m.s. values $\epsilon_{\text{sig},i}$ of all signal modes are identical. Since the singular value is proportional to $1/\lambda_i^2$ the r.m.s. $\epsilon_{\text{nor},i}$ of a normal mode is related to ϵ_{sig} by

$$\epsilon_{\text{nor},i} \propto \frac{\epsilon_{\text{sig}}}{\lambda_i^2} \quad (108)$$

The source for wavefront errors in the form of elastic modes are errors in the support forces of the large monolithic mirrors. For a large number of supports these force errors can be replaced by pressure fields. Since the elastic modes form an orthogonal set of functions and are proportional to the pressure fields generating them, the elastic modes and pressure functions can be regarded as a pair of normal modes similar to the pair of analytical signal and position modes in segmented mirrors. But, instead of being proportional to $1/\lambda_i^2$ the r.m.s. $\epsilon_{\text{ela},i}$ of an elastic mode is, for a given r.m.s. ϵ_{pr} of the pressure field, proportional to $1/\lambda_i^4$:

$$\epsilon_{\text{ela},i} \propto \frac{\epsilon_{\text{pr}}}{\lambda_i^4} \quad (109)$$

A comparison of the equations (108) and (109) shows that the coefficients of the elastic modes generated by random force errors decline much faster with the order of the mode than the coefficients of the normal modes of a segmented mirror generated by signal errors. The difference in the behaviour is, at a first glance, surprising, since the normal modes of a segmented mirror are similar to the elastic modes, that is the relationship between the position modes and the fields of the second derivatives of the position modes is the same. But the difference is that for the normal mirror modes the source is already a kind of curvature field, whereas for the elastic modes there is another additional relationship involving a factor λ_i^2 between the source, which is the pressure field, and the curvature field.

Appendix A : Derivation of elastic modes of a circular plate

For the derivation of the elastic modes of a free circular plate one has to generalise the method introduced in section 2. Instead of equation (9)

$$\langle Lf_i, Lf_j \rangle \propto \delta_{i,j} \quad (110)$$

we require now that

$$\langle Lf_i, Nf_j \rangle \propto \delta_{i,j} \quad (111)$$

with two possibly different differential operators L and N . Partial integration of the left hand side leads to an equation which is equivalent to equation (10) :

$$\langle Lf_i, Nf_j \rangle = \langle N^F Lf_i, f_j \rangle + \underline{\beta}_{L,N}[f_i, f_j] \quad (112)$$

If the boundary functional $\underline{\beta}_{L,N}[f_i, f_j]$ is zero, equations (7), (111), and (112) lead to the linear differential equation

$$N^F Lf_i = \sigma_i^2 f_i \quad (113)$$

For elastic modes the operators are related to the strain and moment tensors. With a prime and an asterix denoting a partial derivative with respect to the radial variable r and the azimuthal variable ϕ , respectively, the components of the strain tensor are defined by

$$\chi_r = -f'', \quad \chi_\phi = -\frac{f'}{r} - \frac{f^{**}}{r^2}, \quad \chi_{r\phi} = -\frac{f'^*}{r} + \frac{f^*}{r^2} \quad (114)$$

and the components of the moment tensor by

$$M_r = D(\chi_r + \nu\chi_\phi), \quad M_\phi = D(\chi_\phi + \nu\chi_r), \quad M_{r\phi} = D(1 - \nu)\chi_{r\phi}, \quad (115)$$

where $D = Kh^2/12$ and $K = Eh/(1 - \nu^2)$. E is the modulus of elasticity, h the mirror thickness, and ν Poisson's ratio. Equation (112) then becomes

$$\begin{aligned} \langle Lf_i, Nf_j \rangle &= \int_0^{2\pi} d\varphi \int_{r_1}^{r_2} dr (M_{r,i}\chi_{r,j} + M_{\phi,i}\chi_{\phi,j} + 2M_{r\phi,i}\chi_{r\phi,j}) \\ &= \int_{r_1}^{r_2} dr [(\chi_{r,i}\chi_{r,j} + \chi_{\phi,i}\chi_{\phi,j} + 2\chi_{r\phi,i}\chi_{r\phi,j}) \\ &\quad + \nu(\chi_{\phi,i}\chi_{r,j} + \chi_{r,i}\chi_{\phi,j} - 2\chi_{r\phi,i}\chi_{r\phi,j})] \\ &\propto \delta_{i,j} \end{aligned} \quad (116)$$

Introducing equation (54) and partial integration lead to the differential equation (72) and a boundary functional. For an arbitrary choice of the functions $f_{n,j}$ the boundary functional is always zero if the following boundary conditions are fulfilled :

$$f_i''(r_x) + \nu \frac{f_i'(r_x)}{r} - n^2 \nu \frac{f_i(r_x)}{r^2} = 0 \quad (117)$$

$$f_i'''(r_x) + \frac{f_i''(r_x)}{r} + (1 + n^2(2 - \nu)) \frac{f_i'(r_x)}{r^2} + n^2(3 - \nu) \frac{f_i(r_x)}{r^3} = 0 \quad (118)$$

for both $r_x = r_1$ and $r_x = r_2$. These four boundary conditions are identical to those for a free thin annular circular plate [3].

Acknowledgements The author would like to thank Gary Chanan for many useful discussions and Ray Wilson and Natalia Yaitskova for critical comments on the manuscript.

References

- 1 Troy, M., Chanan, G., Sirko, E., and Leffert, E., 1998, Residual Misalignments of the Keck Telescope Primary Mirror Segments : Classification of Modes and Implications for Adaptive Optics, *Proceedings of the International Society for Optical Engineering*, Vol. 3352, 307-317
- 2 Noethe, L., Active optics in modern large optical telescopes, *Progress in Optics*, 43, chapter 1
- 3 Noethe, L., 1991, *Journal of Modern Optics*, **38**, 1043-1066
- 4 Cantrill, C.D., 2002, *Modern Mathematical Methods for Physicists and Engineers*, (Cambridge University Press)
- 5 Chanan, G., 2002, Private communication
- 6 Chanan, G., MacMartin, D.G., Nelson, J., Mast, T., Control and Alignment of Segmented-Mirror Telescopes : Matrices, Modes, and Error Propagation, *accepted for publication in Applied Optics*